Rapid Communications

Quantum spiral spin-tensor magnetism

Xiaofan Zhou,[1,2] Xi-Wang Luo,[1] Gang Chen,[2,3,4,*] Suotang Jia,[2,3] and Chuanwei Zhang[1,†]
[1]*Department of Physics, The University of Texas at Dallas, Richardson, Texas 75080, USA*
[2]*State Key Laboratory of Quantum Optics and Quantum Optics Devices, Institute of Laser Spectroscopy, Shanxi University, Taiyuan 030006, China*
[3]*Collaborative Innovation Center of Extreme Optics, Shanxi University, Taiyuan, Shanxi 030006, China*
[4]*Collaborative Innovation Center of Light Manipulations and Applications, Shandong Normal University, Jinan 250358, China*

(Received 22 March 2019; revised manuscript received 18 November 2019; accepted 13 April 2020; published 30 April 2020)

The characterization of quantum magnetism in a large spin ($\geqslant 1$) system naturally involves both spin vectors and spin tensors. While certain types of spin-vector (e.g., ferromagnetic, spiral) and spin-tensor (e.g., nematic in frustrated lattices) orders have been investigated separately, the coexistence and correlation between them have not been well explored. Here, we propose a quantum spiral spin-tensor order on a spin-1 Heisenberg chain subject to a spiral spin-tensor Zeeman field, which can be experimentally realized using a Raman-dressed cold atom optical lattice. We develop a method to fully characterize quantum phases of such spiral tensor magnetism with the coexistence of spin-vector and spin-tensor orders as well as their correlations using eight geometric parameters. Our method provides a powerful tool for characterizing spin-1 quantum magnetism and opens an avenue for exploring magnetic orders and spin-tensor electronics and atomtronics in large-spin systems.

DOI: 10.1103/PhysRevB.101.140412

Introduction. Quantum magnetism originates from the exchange coupling between quantum spins and lies at the heart of many fundamental phenomena in quantum physics [1–3]. In particular, understanding exotic magnetic orders of strongly correlated quantum spin chains is one major issue of modern condensed matter physics. Such interacting many-body systems can give rise to various magnetic orders and the phase transitions between them [4–11]. Major research efforts have been focused on spin-1/2 systems, where collinear (e.g., ferromagnetic and antiferromagnetic) and noncollinear (e.g., spiral) magnetic orders are fully characterized by the spin-vector ($\vec{S}$) configurations, including their local orientations and densities as well as nonlocal correlations [12–22].

Quantum magnetism with large spins, such as spin-1, has also received considerable attention in recent years, where the large spin could originate from, for instance, intrinsic orbital degrees of electrons or pseudospins defined by hyperfine states of cold neutral atoms or ions [23–34]. Mathematically, a full description of a large spin ($\geqslant 1$) involves not only rank-1 spin vectors, but also higher-rank spin tensors, therefore it is expected that the resulting quantum magnetism may possess both spin-vector and spin-tensor orders. So far, the spin-vector magnetism of a strongly correlated spin-1 (or higher) chain has been extensively studied [34–46], and the competition between the spin interaction and Zeeman field (either uniform or spiral along the chain) leads to rich phase diagrams. Certain nematic magnetic orders of spin tensors (with vanishing spin vector) have been investigated in two-dimensional (2D) geometrically frustrated (e.g., triangle) lattices [47–55]. However, magnetic orders with the coexistence of these two orders have not been discovered and a unified description of such magnetic orders is still lacking. Addressing these two important issues should be of great importance for the discovery of different magnetic orders and the exploration of electronics and atomtronics characterized by spin tensors.

We restrict to spin-1 magnetic orders, which may be characterized by two elements: a rank-1 spin vector (represented by an arrow using three parameters) and a rank-2 spin tensor (represented by an ellipsoid using five parameters). In this Rapid Communication, we propose alternative types of quantum spiral spin-tensor orders with the coexistence of spin-vector and spin-tensor orders and develop a geometric method to describe them. Our main results are as follows:

(i) We propose an experimental setup for realizing a spin-1 Heisenberg chain subject to a spiral spin-tensor Zeeman field using a Raman coupled cold atom optical lattice, which can host quantum spiral spin-tensor orders.

(ii) We develop a method for characterizing any spin-1 quantum magnetism with the order parameters and long-range spin correlations described by eight geometric parameters originating from a spin arrow and ellipsoid.

(iii) We obtain the ground-state phase diagram numerically using the density-matrix renormalization group (DMRG) method and showcase its rich physics such as a ferromagnetic spiral tensor phase, where the relative orientation between the spin-vector arrow and spin-tensor ellipsoid exhibits periodic oscillations. In previously studied spiral spin-vector orders [34], the arrow length, ellipsoid size, and their relative orientations are uniformly fixed across the lattice chain, while the 2D nematic phase in a frustrated lattice [47,48] possesses a vanishing spin-vector arrow and fixed ellipsoid size and directions.

*chengang971@163.com
†chuanwei.zhang@utdallas.edu

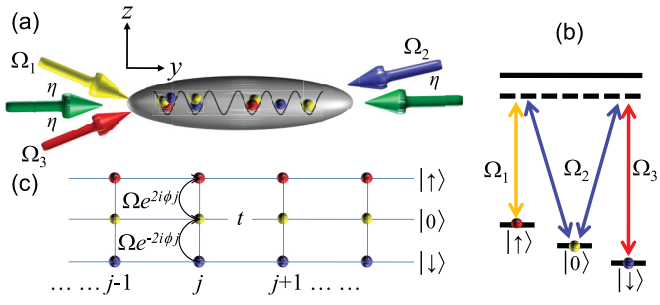

FIG. 1. (a) Schematics of the system setup. Green arrows represent the 1D optical lattice. Yellow, blue, and red arrows represent three Raman lasers. (b) The Raman lasers induce two Raman transitions between spin states $|0\rangle$ and $|\uparrow(\downarrow)\rangle$. (c) Effective description of the model. t is the hopping between neighboring sites, and $\Omega e^{2i\phi j}|0\rangle\langle\uparrow|$ and $\Omega e^{-2i\phi j}|\downarrow\rangle\langle 0|$ are the site-dependent couplings between different spin states.

The model. We consider an experimental setup based on ultracold bosonic atoms in a 1D optical lattice, as shown in Fig. 1(a). Three Raman lasers are used to couple different spin and momentum states [27,56–61]. In particular, a pair of counterpropagating lasers with wavelength λ_L is used to realize the 1D optical lattice $V_{\rm lat}(y) = -V_0\cos^2(k_L y)$ along the y direction, with wave number $k_L = 2\pi/\lambda_L$. All Raman lasers have an angle η with respect to the y direction and they induce two Raman transitions between the spin states $|0\rangle$ and $|\uparrow(\downarrow)\rangle$ [as shown in Fig. 1(b)] with the momentum transfer $2k_{\rm R}$, where $k_{\rm R} = 2\pi\cos(\eta)/\lambda_\Omega$, with λ_Ω the Raman-laser wavelength. Such a Raman-laser setup induces the spin-tensor-momentum coupling [61] for ultracold atomic gases, which has been realized recently in an experiment [62].

The tight-binding Hamiltonian without Raman lasers can be written as $H_0 = -t\sum_{\langle i,j\rangle,\sigma} b^\dagger_{i\sigma}b_{j\sigma} + (U_0/2)\sum_j n_j(n_j-1) + (U_2/2)\sum_j(\mathbf{S}_j^2 - 2n_j)$, where $b^\dagger_{j\sigma}$ ($b_{j\sigma}$) is the creation (annihilation) operator with a spin σ, $n_j = \sum_\sigma b^\dagger_{j\sigma}b_{j\sigma}$ is the density operator, and $\mathbf{S}_j = \sum_{\sigma\acute{\sigma}} b^\dagger_{j\sigma}\mathbf{F}_{\sigma\acute{\sigma}}b_{j\acute{\sigma}}$ with $\mathbf{F}_{\sigma\acute{\sigma}}$ representing the total angular momentum $F = 1$ spin operators and $\sigma = (\uparrow, 0, \downarrow)$. t is the tunneling amplitude between neighboring sites, and U_0 and U_2 are on-site density and spin interaction strengths.

In the Mott limit of commensurate odd integer filling and $U_0, U_2 \gg t$, we can get the effective spin Hamiltonian [63], $H^0_{\rm spin} = \sum_j J_1\mathbf{S}_j\cdot\mathbf{S}_{j+1} + J_2(\mathbf{S}_j\cdot\mathbf{S}_{j+1})^2$. Typically, $J_1 < 0$ for a repulsive interaction, therefore we parametrize J_1 and J_2 on a unit circle with $J_1 = \cos\theta$ and $J_2 = \sin\theta$ and focus on the parameter region $\theta \in [0.5\pi, 1.5\pi]$. For $J_2 > J_1$ (i.e., $0.5 \leqslant \theta/\pi < 1.25$), the system possesses ferromagnetic order, which maximizes $\mathbf{S}_j\cdot\mathbf{S}_{j+1}$ but minimizes $(\mathbf{S}_j\cdot\mathbf{S}_{j+1})^2$ due to the dominating negative bilinear interaction J_1. For a large negative biquadratic interaction $J_2 < J_1$ in the region $(1.25 < \theta/\pi \leqslant 1.5)$, the ground state should maximize $(\mathbf{S}_j\cdot\mathbf{S}_{j+1})^2$ by forming a spin singlet between neighboring sites, which breaks the translational symmetry, leading to the dimer phase [23–25,66]. Typical values for alkaline atoms are $\theta/\pi = 1.26$ for ^{23}Na, 1.15π for ^{7}Li, 1.242 for ^{41}K, and 1.249 for ^{87}Rb [27].

The Raman lasers give rise to the site-dependent spin-flipping terms $\Omega e^{2i\phi j}|0\rangle\langle\uparrow|$ and $\Omega e^{-2i\phi j}|\downarrow\rangle\langle 0|$ [see Fig. 1(c)], which would induce a spiral on-site spin-vector and spin-tensor field. To see this, we write down the tight-binding Hamiltonian for such Raman processes, $H_\Omega = \sqrt{2}\Omega\sum_j(e^{2i\phi j}\hat{b}^\dagger_{j\uparrow}\hat{b}_{j0} + e^{-2i\phi j}\hat{b}^\dagger_{j0}\hat{b}_{j\downarrow} + \text{H.c.})$, where Ω is the Raman coupling strength, and $\phi = \pi\cos(\eta)\lambda_L/\lambda_\Omega$ describes the flux and can be tuned by the angle η. In the Mott limit, H_Ω can be treated as spiral spin-vector and spin-tensor Zeeman fields $H^\Omega_{\rm spin} = 2\Omega\sum_j[\cos(2\phi j)S^x_j - \sin(2\phi j)N^{yz}_j]$, where $N^{\alpha\beta} = \{S^\alpha, S^\beta\}/2 - \delta_{\alpha\beta}\mathbf{S}^2/3$ with $\{\}$ the anticommutation relation and $\alpha(\beta) = (x, y, z)$, Ω is the Zeeman field strength, and ϕ is the spiral period of the field. The total Hamiltonian of our system reads

$$H_{\rm spin} = H^0_{\rm spin} + H^\Omega_{\rm spin}. \tag{1}$$

The competition between the spin interaction $H^0_{\rm spin}$ and spiral on-site field $H^\Omega_{\rm spin}$ may induce many interesting spin-tensor magnetic phases, where both the spin vector and spin tensor have to be considered to fully describe these quantum magnetic orders.

Description of spin-1 magnetic order. The local magnetic order of a spin-1 system can be described by the local densities of eight spin moments (i.e., three spin vectors and five spin tensors). Here, we consider the local spin vector $\vec{S}_j = \left(\langle S^x_j\rangle, \langle S^y_j\rangle, \langle S^z_j\rangle\right)^T$ and the spin-tensor fluctuation matrix T_j whose elements are tensor moments $T^{\alpha\beta}_j = \langle\{S^\alpha_j, S^\beta_j\}\rangle/2 - \langle S^\alpha_j\rangle\langle S^\beta_j\rangle$. Geometrically, $\vec{S}_j$ is characterized by an arrow and T_j by an ellipsoid [with principle axis lengths $l^n_T(j)$ $(n = a, b, c)$ and orientations $\vec{v}^n_T(j)$ given by the square roots of the eigenvalues and eigenvectors of $T^{\alpha\beta}_j$ [67]]. To quantitatively characterize and geometrically visualize the magnetic order, we choose eight independent geometric parameters that could fully describe the spin arrow and ellipsoid: the length l_S and spherical coordinates θ_S, ϕ_S of the arrow, the two axis lengths $l^{a,b}_T$ with the third axis length $l^c_T = \sqrt{2 - (l_S)^2 - (l^a_T)^2 - (l^b_T)^2}$, and orientational Euler angles $\theta_T, \phi_T, \phi'_T$ of the ellipsoid, as shown in Fig. 2(a).

Beside the local densities, the characterization of long-range correlations of the magnetic order requires spin-vector and spin-tensor correlations. In our Heisenberg model, only the same-spin-moment correlations are relevant because of the same-spin-moment interactions, and the correlation function of spin moment $\hat{O}$ over a distance r can be defined as $\mathbb{C}(\hat{O}, r) = (1/L)\sum_j[\langle\hat{O}_j\hat{O}_{j+r}\rangle_\nu - \langle\hat{O}_j\rangle_\nu\langle\hat{O}_{j+r}\rangle_\nu]$, with $\langle\rangle_\nu$ the average value of the ν-fold degenerate ground states. The correlations can have the same geometrical representation as the local densities. The spin-vector correlation is described by an arrow $\vec{\mathbb{S}}_r$ with $\mathbb{S}^\alpha_r = \mathbb{C}(S^\alpha, r)$ and spin arrow lengths S_r, while the spin-tensor correlation $\mathbb{T}_r$ is described by an ellipsoid with the principle axis lengths l^n_r given by the tensor-correlation matrix $\mathbb{T}^{\alpha\beta}_r = \mathbb{C}(N^{\alpha\beta}, r)$.

Spiral spin-tensor magnetism. The numerical ground-state phase diagram of the Hamiltonian (1) can be obtained through the DMRG calculation [68,69], where the length of the spin chain L is up to 96 sites, and we keep the maximum states at 200 and achieve truncation errors of 10^{-8}. The resulting

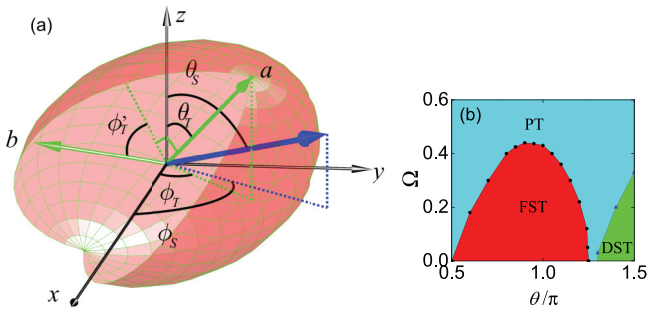

FIG. 2. (a) The description of a spin-1 magnetic order. The blue arrow denotes the spin vector $\vec{S}$, in which θ_S and ϕ_S are the polar angle and azimuth angle with length l_S. The red ellipsoid is the spin tensor T, in which the green arrows are the ellipsoid's orientations $\vec{v}_T^n$ $(n = a, b)$ with the principle axis lengths l_T^n. The Euler angles θ_T, ϕ_T, and ϕ_T' are used to determine the orientation of the ellipsoid, in which θ_T is the polar angle of $\vec{v}_T^a$, ϕ_T is the azimuth angle of $\vec{v}_T^a$, and ϕ_T' is the angle between $\vec{v}_T^b$ and the plane formed by the z axis and $\vec{v}_T^a$. (b) The phase diagram of the Hamiltonian (1) with respect to (θ, Ω) for $\phi/\pi = 1/6$, which includes the paramagnetic tensor (PT), ferromagnetic spiral tensor (FST), and dimer spiral tensor (DST) phases.

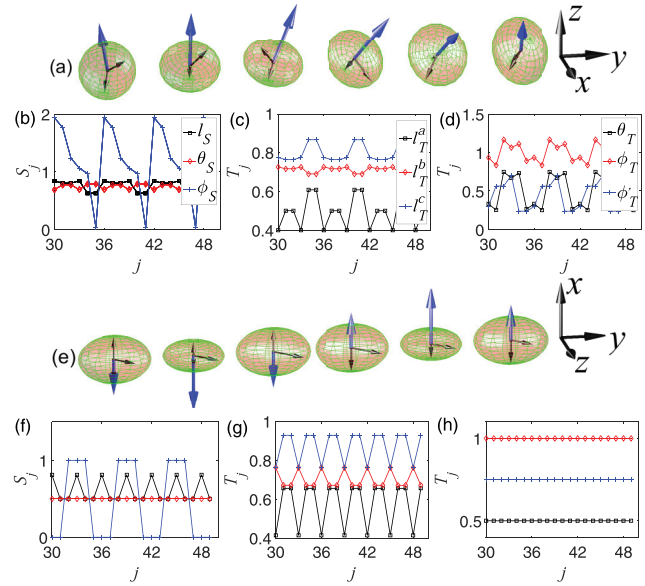

FIG. 3. (a), (e) Schematic diagram of spin-vector density arrows $\vec{S}_j$ and spin-tensor density ellipsoids T_j. (b), (f) Spatial distributions of the spin-vector density arrows $\vec{S}_j$. (c), (d), (g), (h) Spatial distributions of the spin-tensor density ellipsoids T_j. (a)–(d) FST phase with $\theta/\pi = 0.9$ and $\Omega = 0.4$. (e)–(h) PT phase with $\theta/\pi = 0.9$ and $\Omega = 0.5$. $\phi/\pi = 1/6$ for all subfigures.

phase diagram for $\phi/\pi = 1/6$ is plotted in the θ-Ω plane in Fig. 2(b). There are three different phases: the ferromagnetic spiral tensor phase (FST) for $0.5 \leqslant \theta/\pi < 1.25$ and the dimer spiral tensor phase (DST) for $1.25 < \theta/\pi \leqslant 1.5$, both in the small spiral on-site field Ω region, and the paramagnetic tensor phase (PT) for the large Ω. All these phases possess both spiral spin-vector and spin-tensor densities and can be distinguished by spin correlations: (i) For the FST phase, there are spin-vector and spin-tensor long-range correlations with nonzero ferromagnetic order $c_F \equiv \langle S_1^z S_{L/2}^z \rangle$. (ii) For the DST phase, the dimer-vector and dimer-tensor correlations are long range with nonzero dimer order $c_D \equiv \langle D_1^{S^z} D_{L/2}^{S^z} \rangle$ [63]. (iii) For the PT phase, there are no long-range correlations. For other spiral periods ϕ, the quantum phase diagrams are similar, except that the phase transitions may occur at different critical points and the period of the spiral modulation varies in the same way as the spiral period ϕ.

First, we consider the region $0.5\pi \leqslant \theta < 1.25\pi$ with weak Ω (the bottom-left-hand side in the phase diagram), where the spin interactions are still dominant and the ferromagnetic order remains. At $\Omega = 0$, the spin-vector arrow points to a certain direction (assumed to be the z axis) that does not change along the chain, and the spin-tensor ellipsoid is a flat disk in the x-y plane [i.e., $l_T^a = 0, \theta_T = 0$ (i.e., the a axis is parallel to the z axis)] [63]. In the presence of the spiral Zeeman field $(\Omega > 0)$, the spin-vector density arrows $\vec{S}_j$, the spin-tensor density ellipsoids T_j, and their relative orientations become oscillating periodically along the chain, forming spiral loops in the Bloch sphere [63] and leading to the FST phase, where the local spiral magnetism and long-range correlations coexist. Figure 3(a) shows the arrows $\vec{S}_j$ and ellipsoids T_j in one spatial period, which possess a spiral structure.

For the quantitative characterization of the spiral tensor order, we plot the spatial distributions of $[l_S(j), \theta_S(j), \phi_S(j)]$ for the vector-density arrows, the principle axis lengths $[l_T^a(j), l_T^b(j), l_T^c(j)]$, and the orientational Euler angles $[\theta_T(j), \phi_T(j), \phi_T'(j)]$ of the ellipsoids in Figs. 3(b)–3(d). We find $l_S(j)$, $\theta_S(j)$, and $\phi_S(j)$ oscillate along the chain with the same period as the spiral field, and $\phi_S(j)$ changes from 0 to 2π during one period [see Fig. 3(b)]. Correspondingly, the arrows $\vec{S}_j$ within one period form a circular loop around the z axis [63]. For the spin-tensor density ellipsoids T_j, besides the modulation in its size $l_T^n(j)$ [see Fig. 3(c)], the corresponding axes form a twisted loop (figure-8 shaped) [63], leading to relative rotations between the spin-vector density arrows and spin-tensor density ellipsoids [$\theta_T(j)$, $\phi_T(j)$, and $\phi_T'(j)$ oscillate differently from $\theta_S(j), \phi_S(j)$], as shown in Fig. 3(d). Such a spiral magnetic configuration originates from the competition between the on-site spin-vector potential $[\cos(2\phi j) S_j^x]$ and spin-tensor potential $[-\sin(2\phi j) N_j^{yz}]$. Without the spin-tensor field (i.e., only spin-vector field), the spin-vector density arrows and spin-tensor density ellipsoids would rotate similarly with a fixed relative orientation [i.e., $\theta_T(j)$-$\theta_S(j)$, $\phi_T(j)$-$\phi_S(j)$, and $\phi_T'(j)$ uniform along the chain], and all ellipsoids would have a fixed size [i.e., $l_T^n(j)$ uniform along the chain] [63]. Moreover, the ferromagnetic spiral order is characterized by the long-range correlation of both spin vector $\vec{\mathbb{S}}_r$ and spin tensor $\mathbb{T}_r$ [63].

As we increase Ω, the spin-vector rotation loop in a period first enlarges and then shrinks to a narrow ellipse (cigar shaped). For strong Ω, the system undergoes a second-order phase transition from the FST phase to the PT phase, where the long-range correlations and ferromagnetic order c_F vanish [see Fig. 4(c)]. In the PT phase, the on-site Zeeman field in Hamiltonian (1) dominates, and all spin-vector density arrows are parallel to the Zeeman field $[\cos(2\phi j) S_j^x]$ with length modulations. The corresponding local magnetic densities are

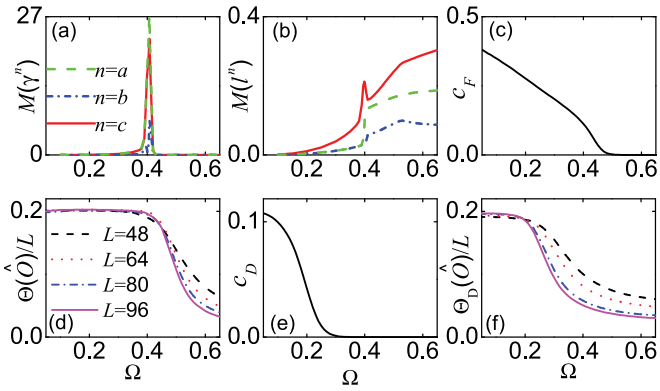

FIG. 4. (a)–(c) Oscillation amplitude of angles $M(\gamma^n)$, lengths $M(l^n)$, and ferromagnetic order c_F as a function of Ω. (d) The correlation lengths $\Theta(\hat{O})/L$ as functions of Ω for different lattice lengths L. (e) Dimer order c_D as a function of Ω. (f) Dimer correlation lengths $\Theta_{\rm D}(\hat{O})/L$ as functions of Ω for different L, with $\theta/\pi = 1.4$. In (d) and (f), we only plot $\hat{O} = S^z$ as an example (others are shown in the Supplemental Material [63]). $\theta/\pi = 0.9$ in (a)–(d), $L = 96$ in (a)–(c) and (e). Common parameter $\phi/\pi = 1/6$.

shown in Fig. 3(e). Clearly, the spin-vector density loop shrinks into a line on the x axis in the PT phase ($\theta_S = \pi/2$ and $\phi_S = 0, \pi$).

The rotation loop of the tensor ellipsoids changes similarly as we increase Ω: The loop first enlarges then shrinks into a line after the phase transition, where only the sizes $l_T^n(j)$ (not the direction) of the ellipsoids oscillate [63], as shown in Figs. 3(g) and 3(h). The oscillation of $l_T^n(j)$ makes the PT phase different from a regular paramagnetic phase. In the PT phase, the vector correlation arrows $\vec{\mathbb{S}}_r$ and tensor correlation ellipsoids $\mathbb{T}_r$ decay exponentially (in size) with the distance r, indicating that there does not exist any long-range order [63].

Now we turn to the parameter region $1.25 < \theta/\pi \leqslant 1.5$. The system still stays in the PT phase for a large Ω. For a small Ω, the negative biquadratic interaction dominates, leading to the second-order phase transition to the DST phase. In this phase, the local spin-vector and spin-tensor densities behave similarly as in the PT phase, forming lines instead of spiral loops [63]. Interestingly, there exist spiral loops for the dimer-vector densities $\mathrm{D}_j^{\vec{S}}$ and dimer-tensor densities D_j^{T} [63], owing to the presence of the on-site spin-tensor field. The ordinary correlations of both spin vector $\vec{\mathbb{S}}_r$ and spin tensor $\mathbb{T}_r$ decay similarly as the PT phase [63]. However, there exist long-range correlations for both dimer vector $\mathbb{D}_r^{\vec{S}}$ and dimer tensor $\mathbb{D}_r^{T}$ [63], and the dimer order c_D emerges.

Phase transitions. The phase transitions between the above phases can be characterized by the critical behaviors of the local densities and the correlations of the spin vectors and spin tensors. When Ω increases from zero, the spiral loops of the spin-vector density arrows $\vec{S}_j$ and the spin-tensor density ellipsoids' axes emerge from an initial uniform distribution, become larger, then shrink, and finally disappear at the phase transition [63]. The spin-tensor density ellipsoids T_j have two critical behaviors when crossing the phase transition: (i) The angles $\gamma_j^n = \vec{S}_j \angle \vec{v}_T^n(j)$ show a large oscillation in real space, which can be characterized by a sharp peak for the oscillatory amplitude of angles $M(\gamma^n) = \max(\gamma_j^n) - \min(\gamma_j^n)$ located at the phase boundary, as clearly shown in Fig. 4(a). (ii) The oscillatory amplitude of the ellipsoid's axis lengths $M(l_T^n) = \max[l_T^n(j)] - \min[l_T^n(j)]$ have sharp features at the critical point, as shown in Fig. 4(b). In addition, the ferromagnetic order c_F decreases and vanishes across the phase transition, as shown in Fig. 4(c).

The transition from the PT to FST or DST phases corresponds to the formation of long-range order, therefore the transition should also be captured by more essential correlation lengths. The numerical results for the spin-vector (spin-tensor) correlation length $\Theta(\hat{O}) = \sqrt{\frac{\sum_{j\neq L/2}(j-L/2)^2\langle \hat{O}_j \hat{O}_{L/2}\rangle}{2\sum_{j\neq L/2}\langle \hat{O}_j \hat{O}_{L/2}\rangle}}$ [70] ($\hat{O} = S^{y,z}, T^{yy,zz,xy,xz}$) for the transition between PT and FST phases are shown in Fig. 4(d), which show that there are (no) spin-vector and spin-tensor long-range correlations for the FST (PT) phase. The critical point Ω_c in the thermodynamic limit is determined by the crossing point between the $\Theta(\hat{O})/L$ curves for different finite lattice lengths, as shown in Fig. 4(d).

Similarly, Figs. 4(e) and 4(f) show the dimer-order c_D and dimer-vector (dimer-tensor) correlation length $\Theta_{\rm D}(\hat{O})/L$ for finite lattice lengths, where $\Theta_{\rm D}(\hat{O}) = \Theta(D_{\hat{O}})$ ($\hat{O} = S^{x,y,z}, T^{xx,yy,zz,xy,xz,yz}$) is used to determine the critical point between the PT and DST phases. The dimer correlation length of a finite lattice length retains and then decays. In the decaying region, the dimer correlation lengths of several finite lattices cross at one point. In the process of increasing Ω, the dimer-vector (dimer-tensor) density spiral loop emerges from a uniform distribution, becomes larger, then shrinks, and finally disappears [63].

Discussion and conclusions. The phase transition is related with the symmetry of the Hamiltonian. For instance, in the FST phase, the ground state is fourfold degenerate due to spontaneous symmetry breaking of the Z_2 exchange symmetry $S^y \leftrightarrow S^z$ and Z_2 reflection symmetry $S^{y(z)} \leftrightarrow -S^{y(z)}$ of the Hamiltonian (1), leading to nonzero $\langle S^z\rangle$ and $\langle S^y\rangle$. However, in the PT phase, the ground state is nondegenerate, yielding $\langle S^z\rangle = 0$ and $\langle S^y\rangle = 0$, thus the spiral loop shrinks into a line (l_S oscillate, $\theta_S = \pi/2$, $\phi_S = 0, \pi$) [see Fig. 3(f)].

Finally, we remark that the local spin states are mixed states for the strongly correlated spin chain, therefore another useful representation of higher-spin pure states, Majorana stars [27,71–75], is not suitable for studying correlated quantum magnetism.

In summary, we propose an alternative type of quantum magnetism, the spiral spin-tensor order, in a spin-1 Heisenberg chain subject to a spiral spin-tensor Zeeman field. We characterize such quantum spiral spin-tensor orders and their phase transitions using local spin-vector and spin-tensor densities and their correlations, which can be visualized using eight geometric parameters. To detect such magnetic orders, we can isolate the sites of interest using additional site-resolved potentials and measure their local spin states and nonlocal spin correlations [12–15]. Our method can also be used to describe spin-1 quantum magnetism formed by a trapped ion array with tunable long-range interactions [33]. Our work should lay the foundation for exploring strongly correlated quantum magnetism in a large spin system and pave the way for engineering different types of spin-tensor electronic and atomtronic devices.

Acknowledgments. X.Z., G.C., and S.J. are supported by National Key R&D Program of China under Grant No. 2017YFA0304203, the NSFC under Grants No. 11674200 and No. 11804204, and 1331KSC. X.L. and C.Z. are supported by AFOSR (FA9550-16-1-0387), ARO (W911NF-17-1-0128), and NSF (PHY-1806227),

[1] A. Auerbach, *Interacting Electrons and Quantum Magnetism* (Springer, New York, 1994).
[2] U. Schollwöck, J. Richter, D. J. J. Farnell, and R. F. Bisho, *Quantum Magnetism* (Springer, New York, 2008).
[3] S. Sachdev, Quantum magnetism and criticality, Nat. Phys. **4**, 173 (2008).
[4] I. Dzyaloshinskii, A thermodynamic theory of weak ferromagnetism of antiferromagnetics, J. Phys. Chem. Solids **4**, 241 (1958).
[5] T. Moriya, Anisotropic superexchange interaction and weak ferromagnetism, Phys. Rev. **120**, 91 (1960).
[6] E. Manousakis, The spin-1/2 Heisenberg antiferromagnet on a square lattice and its application to the cuprous oxides, Rev. Mod. Phys. **63**, 1 (1991).
[7] F. D. M. Haldane, Nonlinear Field Theory of Large-Spin Heisenberg Antiferromagnets: Semiclassically Quantized Solitons of the One-Dimensional Easy-Axis Néel State, Phys. Rev. Lett. **50**, 1153 (1983).
[8] I. Affleck and F. D. M. Haldane, Critical theory of quantum spin chains, Phys. Rev. B **36**, 5291 (1987).
[9] I. Affleck, T. Kennedy, E. H. Lieb, and H. Tasaki, Rigorous Results on Valence-Bond Ground States in Antiferromagnets, Phys. Rev. Lett. **59**, 799 (1987).
[10] R. Islam, C. Senko, W. C. Campbell, S. Korenblit, J. Smith, A. Lee, E. E. Edwards, C.-C. J. Wang, J. K. Freericks, and C. Monroe, Emergence and frustration of magnetic order with variable-range interactions in a trapped ion quantum simulator, Science **340**, 583 (2013).
[11] K. D. McAlpine, S. Paganelli, S. Ciuchi, A. Sanpera, and G. D. Chiara, Magnetic phases of spin-1 lattice gases with random interactions, Phys. Rev. B **95**, 235128 (2017).
[12] J. Simon, W. S. Bakr, R. Ma, M. E. Tai, P. M. Preiss, and M. Greiner, Quantum simulation of antiferromagnetic spin chains in an optical lattice, Nature (London) **472**, 307 (2011).
[13] M. F. Parsons, A. Mazurenko, C. S. Chiu, G. Ji, D. Greif, and M. Greiner, Site-resolved measurement of the spin-correlation function in the Fermi-Hubbard model, Science **353**, 1253 (2016).
[14] A. Mazurenko, C. S. Chiu, G. Ji, M. F. Parsons, M. Kanász-Nagy, R. Schmidt, F. Grusdt, E. Demler, D. Greif, and M. Greiner, A cold-atom Fermi-Hubbard antiferromagnet, Nature (London) **545**, 462 (2017).
[15] M. Boll, T. A. Hilker, G. Salomon, A. Omran, J. Nespolo, L. Pollet, I. Bloch, and C. Gross, Spin- and density-resolved microscopy of antiferromagnetic correlations in Fermi-Hubbard chains, Science **353**, 1257 (2016).
[16] D. Greif, T. Uehlinger, G. Jotzu, L. Tarruell, and T. Esslinger, Short-range quantum magnetism of ultracold fermions in an optical lattice, Science **340**, 1307 (2013).
[17] R. A. Hart, P. M. Duarte, T.-L. Yang, X. Liu, T. Paiva, E. Khatami, R. T. Scalettar, N. Trivedi, D. A. Huse, and R. G. Hulet, Observation of antiferromagnetic correlations in the Hubbard model with ultracold atoms, Nature (London) **519**, 211 (2015).
[18] Z. Cai, X. Zhou, and C. Wu, Magnetic phases of bosons with synthetic spin-orbit coupling in optical lattices, Phys. Rev. A **85**, 061605 (2012).
[19] Z. Cai, H. Hung, L. Wang, and C. Wu, Quantum magnetic properties of the $SU(2N)$ Hubbard model in the square lattice: A quantum Monte Carlo study, Phys. Rev. B **88**, 125108 (2013).
[20] W. Yang, J. Wu, S. Xu, Z. Wang, and C. Wu, One-dimensional quantum spin dynamics of Bethe string states, Phys. Rev. B **100**, 184406 (2019).
[21] Z. Wang, J. Wu, W. Yang, A. K. Bera, D. Kamenskyi, A. T. M. N. Islam, S. Xu, J. M. Law, B. Lake, C. Wu, and A. Loidl, Experimental observation of Bethe strings, Nature (London) **554**, 219 (2018).
[22] G. Salomon, J. Koepsell, J. Vijayan, T. A. Hilker, J. Nespolo, L. Pollet, I. Bloch, and C. Gross, Direct observation of incommensurate magnetism in Hubbard chains, Nature (London) **565**, 56 (2019).
[23] S. R. White and D. A. Huse, Numerical renormalization-group study of low-lying eigenstates of the antiferromagnetic $S = 1$ Heisenberg chain, Phys. Rev. B **48**, 3844 (1993).
[24] J. J. García-Ripoll, M. A. Martin-Delgado, and J. I. Cirac, Implementation of Spin Hamiltonians in Optical Lattices, Phys. Rev. Lett. **93**, 250405 (2004)
[25] M. Rizzi, D. Rossini, G. De Chiara, S. Montangero, and R. Fazio, Phase Diagram of Spin-1 Bosons on One-Dimensional Lattices, Phys. Rev. Lett. **95**, 240404 (2005).
[26] C. D. Hamley, C. S. Gerving, T. M. Hoang, E. M. Bookjans, and M. S. Chapman, Spin-nematic squeezed vacuum in a quantum gas, Nat. Phys. **8**, 305 (2012).
[27] D. M. Stamper-Kurn and M. Ueda, Spinor Bose gases: Symmetries, magnetism, and quantum dynamics, Rev. Mod. Phys. **85**, 1191 (2013).
[28] M. Piraud, Z. Cai, I. P. McCulloch, and U. Schollwöck, Quantum magnetism of bosons with synthetic gauge fields in one-dimensional optical lattices: A density-matrix renormalization-group study, Phys. Rev. A **89**, 063618 (2014).
[29] S. S. Natu, X. Li, and W. S. Cole, Striped ferronematic ground states in a spin-orbit-coupled $S = 1$ Bose gas, Phys. Rev. A **91**, 023608 (2015).
[30] D. Campbell, R. Price, A. Putra, A. Valdés-Curiel, D. Trypogeorgos, and I. B. Spielman, Magnetic phases of spin-1 spin-orbit-coupled Bose gases, Nat. Commun. **7**, 10897 (2016).
[31] G. Martone, F. Pepe, P. Facchi, S. Pascazio, and S. Stringari, Tricriticalities and Quantum Phases in Spin-Orbit-Coupled Spin-1 Bose Gases, Phys. Rev. Lett. **117**, 125301 (2016).
[32] E. J. König and J. H. Pixley, Quantum Field Theory of Nematic Transitions in Spin-Orbit-Coupled Spin-1 Polar Bosons, Phys. Rev. Lett. **121**, 083402 (2018).
[33] C. Senko, P. Richerme, J. Smith, A. Lee, I. Cohen, A. Retzker, and C. Monroe, Realization of a Quantum Integer-Spin Chain with Controllable Interactions, Phys. Rev. X **5**, 021026 (2015).

[34] J. H. Pixley, W. S. Cole, I. B. Spielman, M. Rizzi, and S. D. Sarma, Strong-coupling phases of the spin-orbit-coupled spin-1 Bose-Hubbard chain: Odd-integer Mott lobes and helical magnetic phases, Phys. Rev. A **96**, 043622 (2017).

[35] J. Lou, X. Dai, S. Qin, Z. Su, and L. Yu, Heisenberg spin-1 chain in a staggered magnetic field: A density-matrix-renormalization-group study, Phys. Rev. B **60**, 52 (1999).

[36] J. Lou, C. Chen, J. Zhao, X. Wang, T. Xiang, Z. Su, and L. Yu, Midgap States in Antiferromagnetic Heisenberg Chains with a Staggered Field, Phys. Rev. Lett. **94**, 217207 (2005).

[37] M. Hagiwara, L. P. Regnault, A. Zheludev, A. Stunault, N. Metoki, T. Suzuki, S. Suga, K. Kakurai, Y. Koike, P. Vorderwisch, and J.-H. Chung, Spin Excitations in an Anisotropic Bond-Alternating Quantum $S = 1$ Chain in a Magnetic Field: Contrast to Haldane Spin Chains, Phys. Rev. Lett. **94**, 177202 (2005).

[38] S. R. Manmana, A. M. Läuchli, F. H. L. Essler, and F. Mila, Phase diagram and continuous pair-unbinding transition of the bilinear-biquadratic $S = 1$ Heisenberg chain in a magnetic field, Phys. Rev. B **83**, 184433 (2011).

[39] G. D. Chiara, M. Lewenstein, and A. Sanpera, Bilinear-biquadratic spin-1 chain undergoing quadratic Zeeman effect, Phys. Rev. B **84**, 054451 (2011).

[40] K. Rodríguez, A. Argüelles, A. K. Kolezhuk, L. Santos, and T. Vekua, Field-Induced Phase Transitions of Repulsive Spin-1 Bosons in Optical Lattices, Phys. Rev. Lett. **106**, 105302 (2011).

[41] M. Weyrauch and M. V. Rakov, Dimerization in ultracold spinor gases with Zeeman splitting, Phys. Rev. B **96**, 134404 (2017).

[42] M. Hermele, V. Gurarie, and A. M. Rey, Mott Insulators of Ultracold Fermionic Alkaline Earth Atoms: Underconstrained Magnetism and Chiral Spin Liquid, Phys. Rev. Lett. **103**, 135301 (2009).

[43] A. V. Gorshkov, M. Hermele, V. Gurarie, C. Xu, P. S. Julienne, J. Ye, P. Zoller, E. Demler, M. D. Lukin, and A. M. Rey, Two-orbital SU(N) magnetism with ultracold alkaline-earth atoms, Nat. Phys. **6**, 289 (2010).

[44] S. R. Manmana, K. R. A. Hazzard, G. Chen, A. E. Feiguin, and A. M. Rey, SU(N) magnetism in chains of ultracold alkaline-earth-metal atoms: Mott transitions and quantum correlations, Phys. Rev. A **84**, 043601 (2011).

[45] B. Yan, S. A. Moses, B. Gadway, J. P. Covey, K. R. A. Hazzard, A. M. Rey, D. S. Jin, and J. Ye, Observation of dipolar spin-exchange interactions with lattice-confined polar molecules, Nature (London) **501**, 521 (2013).

[46] X. Zhang, M. Bishof, S. L. Bromley, C. V. Kraus, M. S. Safronova, P. Zoller, A. M. Rey, and J. Ye, Spectroscopic observation of SU(N)-symmetric interactions in Sr orbital magnetism, Science **345**, 1467 (2014).

[47] H. Tsunetsugu and M. Arikawa, Spin nematic phase in $S = 1$ triangular antiferromagnets, J. Phys. Soc. Jpn. **75**, 083701 (2006).

[48] A. Läuchli, F. Mila, and K. Penc, Quadrupolar Phases of the $S = 1$ Bilinear-Biquadratic Heisenberg Model on the Triangular Lattice, Phys. Rev. Lett. **97**, 087205 (2006).

[49] S. Bhattacharjee, V. B. Shenoy, and T. Senthil, Possible ferro-spin nematic order in $NiGa_2S_4$, Phys. Rev. B **74**, 092406 (2006).

[50] J.-H. Park, S. Onoda, N. Nagaosa, and J. H. Han, Nematic and Chiral Order for Planar Spins on a Triangular Lattice, Phys. Rev. Lett. **101**, 167202 (2008)

[51] R. K. Kaul, Spin nematic ground state of the triangular lattice $S = 1$ biquadratic model, Phys. Rev. B **86**, 104411 (2012).

[52] C. Xu, F. Wang, Y. Qi, L. Balents, and M. P. A. Fisher, Spin Liquid Phases for Spin-1 Systems on the Triangular Lattice, Phys. Rev. Lett. **108**, 087204 (2012).

[53] T. A. Tóth, A. M. Läuchli, F. Mila, and K. Penc, Competition between two- and three-sublattice ordering for $S = 1$ spins on the square lattice, Phys. Rev. B **85**, 140403 (2012)

[54] A. Smerald and N. Shannon, Theory of spin excitations in a quantum spin-nematic state, Phys. Rev. B **88**, 184430 (2013).

[55] R. Yu and Q. Si, Antiferroquadrupolar and Ising-Nematic Orders of a Frustrated Bilinear-Biquadratic Heisenberg Model and Implications for the Magnetism of FeSe, Phys. Rev. Lett. **115**, 116401 (2015).

[56] J. Dalibard, F. Gerbier, G. Juzeliūnas, and P. Öhberg, Colloquium: Artificial gauge potentials for neutral atoms, Rev. Mod. Phys. **83**, 1523 (2011).

[57] N. Goldman, G. Juzeliūnas, P. Öhberg, and I. B. Spielman, Light-induced gauge fields for ultracold atoms, Rep. Prog. Phys. **77**, 126401 (2014).

[58] Y.-J. Lin, K. Jiménez-García, and I. B. Spielman, Spin-orbit-coupled Bose-Einstein condensates, Nature (London) **471**, 83 (2011).

[59] V. Galitski and I. B. Spielman, Spin-orbit coupling in quantum gases, Nature (London) **494**, 49 (2013).

[60] H. Zhai, Degenerate quantum gases with spin-orbit coupling: A review, Rep. Prog. Phys. **78**, 026001 (2015).

[61] X.-W. Luo, K. Sun, and C. Zhang, Spin-Tensor–Momentum-Coupled Bose-Einstein Condensates, Phys. Rev. Lett. **119**, 193001 (2017).

[62] D. Li, L. Huang, P. Peng, G. Bian, P. Wang, Z. Meng, L. Chen, and J. Zhang, Experimental realization of a spin-tensor momentum coupling in ultracold Fermi gases, arXiv:2003.11829.

[63] See Supplemental Material at http://link.aps.org/supplemental/10.1103/PhysRevB.101.140412 for details of the derivation of Hamiltonian Eq. (1), spin-vector and spin-tensor magnetic orders, the results due to the spin-vector potential, dimer spiral tensor phase, correlation lengths near phase transitions, and the magnetic order with a spin-tensor interaction, which includes Refs. [64,65].

[64] J. R. Schrieffer and P. A. Wolff, Relation between the Anderson and Kondo Hamiltonians, Phys. Rev. **149**, 491 (1966).

[65] A. Imambekov, M. Lukin, and E. Demler, Spin-exchange interactions of spin-one bosons in optical lattices: Singlet, nematic, and dimerized phases, Phys. Rev. A **68**, 063602 (2003).

[66] S. K. Yip, Dimer State of Spin-1 Bosons in an Optical Lattice, Phys. Rev. Lett. **90**, 250402 (2003).

[67] H. M. Bharath, Non-Abelian geometric phases carried by the spin fluctuation tensor, J. Math. Phys. **59**, 062105 (2018).

[68] S. R. White, Density Matrix Formulation for Quantum Renormalization Groups, Phys. Rev. Lett. **69**, 2863 (1992).

[69] U. Schollwök, The density-matrix renormalization group, Rev. Mod. Phys. **77**, 259 (2005).

[70] M. Campostrini, A. Pelissetto, and E. Vicari, Finite-size scaling at quantum transitions, Phys. Rev. B **89**, 094516 (2014).

[71] E. Majorana, Atomi orientati in campo magnetico variabile, Nuovo Cimento **9**, 43 (1932).

[72] J. H. Hannay, The Berry phase for spin in the Majorana representation, J. Phys. A **31**, L53 (1998).

[73] B. Lian, T.-L. Ho, and H. Zhai, Searching for non-Abelian phases in the Bose-Einstein condensate of dysprosium, Phys. Rev. A **85**, 051606 (2012).

[74] X. Cui, B. Lian, T.-L. Ho, B. L. Lev, and H. Zhai, Synthetic gauge field with highly magnetic lanthanide atoms, Phys. Rev. A **88**, 011601 (2013).

[75] H. D. Liu and L. B. Fu, Representation of Berry Phase by the Trajectories of Majorana Stars, Phys. Rev. Lett. **113**, 240403 (2014).